Graphene Anchored with Co_3O_4 Nanoparticles as Anode of Lithium Ion Batteries with Enhanced Reversible Capacity and Cyclic Performance

Zhong-Shuai Wu, Wencai Ren,* Lei Wen, Libo Gao, Jinping Zhao, Zongping Chen, Guangmin Zhou, Feng Li, and Hui-Ming Cheng*

Shenyang National Laboratory for Materials Science, Institute of Metal Research, Chinese Academy of Sciences, 72 Wenhua Road, Shenyang 110016, People's Republic of China

ABSTRACT We report a facile strategy to synthesize the nanocomposite of Co_3O_4 nanoparticles anchored on conducting graphene as an advanced anode material for high-performance lithium-ion batteries. The Co_3O_4 nanoparticles obtained are 10−30 nm in size and homogeneously anchor on graphene sheets as spacers to keep the neighboring sheets separated. This Co_3O_4/graphene nanocomposite displays superior Li-battery performance with large reversible capacity, excellent cyclic performance, and good rate capability, highlighting the importance of the anchoring of nanoparticles on graphene sheets for maximum utilization of electrochemically active Co_3O_4 nanoparticles and graphene for energy storage applications in high-performance lithium-ion batteries.

KEYWORDS: graphene · cobalt oxide · nanomaterial · anode · lithium-ion batteries · cyclic performance

Lithium-ion batteries (LIBs) are the power source of choice not only for popular consumer electronics but also for upcoming electric vehicles.[1−3] So far, various materials, such as graphitic/non-graphitic carbon,[4] transition-metal oxides (SnO_2,[5] TiO_2,[6] Fe_2O_3,[7] Co_3O_4,[8−10] NiO,[11] MnO_2,[12] MoO_3,[13] WO_3[14]), chalcogenides (TiS_2),[15,16] nitrides,[17] polymers,[18] lithium alloys (Si, Sn, Al, Sb)/multinary alloys,[19−21] and their composites,[22−26] have been exploited as the anode materials of LIBs. Among them, Co_3O_4 attracts extensive interest for LIBs due to its high theoretical capacity (890 mAh g^{-1}), more than two times larger than that of graphite (372 mAh g^{-1}), which are expected to meet the requirements of future energy storage systems.[8−10] However, its large volume expansion/contraction and severe particle aggregation associated with the Li^+ insertion and extraction process lead to electrode pulverization and loss of interparticle contact and, consequently, result in a large irreversible capacity loss and poor cycling stability.[27,28] A variety of appealing strategies have been utilized to solve these intractable problems, including the use of carbon-based nanocomposites[28−32] and unique Co_3O_4 nanostructures/microstructures of nanotubes,[9] nanowires,[27] nanoparticles (NPs),[33] nanorods,[34] octahedral cages,[35] and plates.[10] However, to keep large reversible capacity combined with high Coulombic efficiency, achieving long cycling life and good rate capability of Co_3O_4 electrode material still remains a great challenge.

Graphene, a new two-dimensional carbon material, is recently expected to be an advanced anode material in LIBs[36−45] due to its superior electrical conductivity, high surface-to-volume ratio, ultrathin thickness, structural flexibility, and chemical stability.[46−50] It has been demonstrated that graphene-based anode materials have large initial discharge capacity (600−2042 mAh g^{-1}) and reversible capacity (540−1264 mAh g^{-1}), although they suffer from large irreversible capacity, low initial Coulombic efficiency, and fast capacity fading.[36−40] More importantly, graphene can also be used in composites with metallic or oxide NPs to improve the electrochemical performance of these particles[40−44] because the ultrathin flexible graphene layers not only can provide a support for anchoring well-dispersed NPs and work as a highly conductive matrix for enabling good contact between them[51] but also can effectively prevent the volume expansion/contraction and aggregation of NPs during Li charge/discharge process.[40] Meanwhile, the anchoring of NPs on graphene can effectively reduce the degree of restacking of graphene sheets and consequently

*Address correspondence to cheng@imr.ac.cn, wcren@imr.ac.cn.

Received for review April 10, 2010 and accepted May 02, 2010.

Published online May 10, 2010. 10.1021/nn100740x

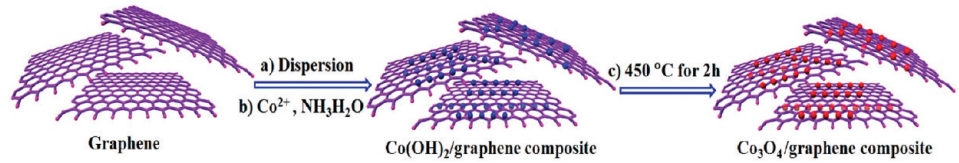

Figure 1. Schematic representation of the fabrication process of Co_3O_4/graphene composite. (a) Dispersion of chemically derived graphene in isopropyl alcohol−water (1:1, v/v) solution. (b) Formation of $Co(OH)_2$/graphene composite in basic solution. (c) Phase transformation from $Co(OH)_2$/graphene composite to Co_3O_4/graphene composite by calcination.

keep their high active surface area and, to some extent, increase the lithium storage capacity and cyclic performance of graphene-based material.[36,40−43] It is well-accepted that nanomaterials have advantages of good cycling performance and short path length for Li^+ transport over their bulk counterparts due to the large contact area between electrode and electrolyte.[3,52] Therefore, it is believed that the composite of flexible and electrically conductive graphene anchored with nanostructured Co_3O_4 particles can efficiently utilize the combinative merits of nanosized Co_3O_4 and graphene and obtain LIBs with superior performance.

Herein, we report a facile strategy to synthesize such composite of Co_3O_4 NPs anchored on conducting graphene as an advanced anode material for high-performance LIBs. The Co_3O_4 NPs obtained are 10−30 nm in size and homogeneously anchor on graphene sheets as spacers to keep the neighboring sheets separated. This Co_3O_4/graphene nanocomposite displays superior LIB performance with large reversible capacity, high Coulombic efficiency, excellent cyclic performance, and good rate capability, highlighting the importance of the anchoring of NPs on graphene sheets for maximum utilization of electrochemically active Co_3O_4 NPs and graphene for energy storage applications in high-performance LIBs.

RESULTS AND DISCUSSION

Figure 1 illustrates the preparation of single-crystalline Co_3O_4 NPs anchored on graphene by solution-phase dispersion of Co^{2+} inorganic salt on graphene in basic ($NH_3 \cdot H_2O$) aqueous solution and subsequent transformation of $Co(OH)_2$/graphene into Co_3O_4/graphene composite by calcination at 450 °C. Figure 2a shows the typical X-ray diffraction (XRD) pattern of the as-prepared Co_3O_4/graphene composite. Compared to that of pure Co_3O_4 (Figure S1 in the Supporting Information), an additional small and low broad (002) diffraction peak appears at 2θ of 24.5−27.5°, which can be indexed into the disorderedly stacked graphene sheets (Figure S2).[53] Moreover, this broad peak is weaker than that of the as-prepared graphene (Figure S2), suggestive of more disordered stacking and

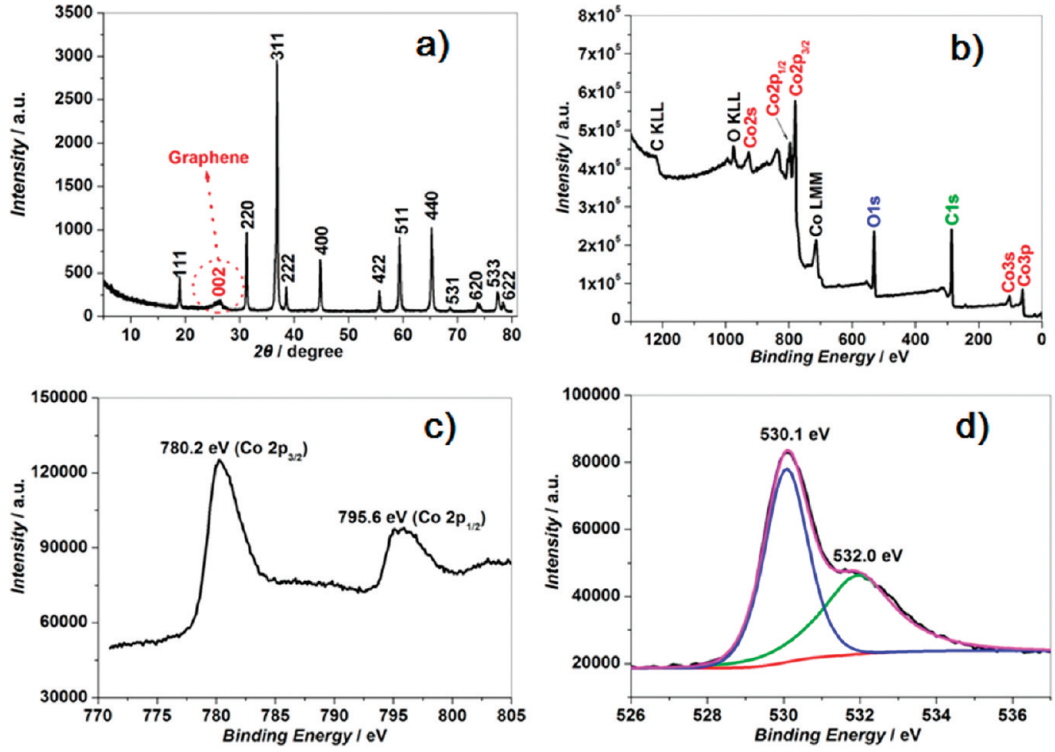

Figure 2. Powder XRD pattern (a) and XPS spectrum (b) of Co_3O_4/graphene composite. Co 2p (c) and O 1s (d) XPS spectra of Co_3O_4/graphene composite. The red dot circle in (a) indicates the (002) diffraction peak of graphene sheets in the Co_3O_4/graphene composite.

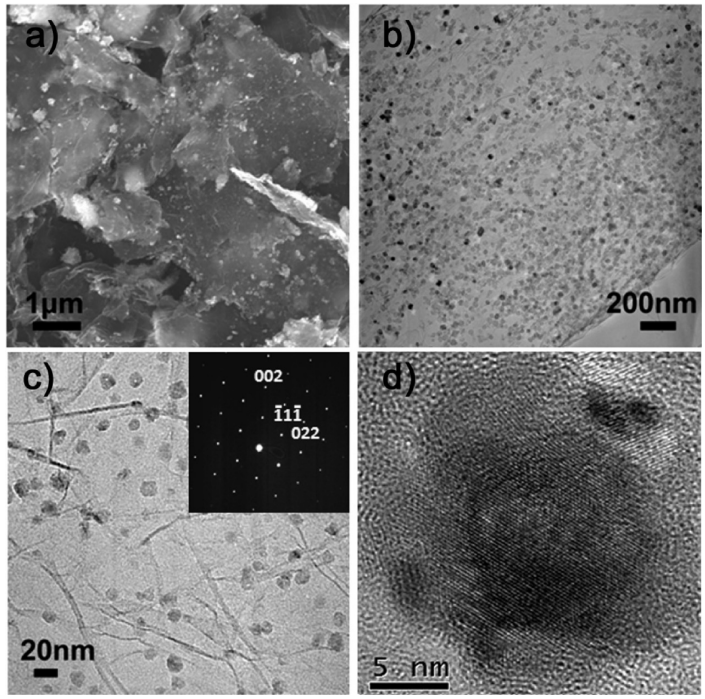

Figure 3. (a) SEM image of Co_3O_4/graphene composite. (b) Low-magnification TEM, (c) high-magnification TEM, and (d) HR-TEM images of Co_3O_4/graphene composite. The inset in (c) is the SAED pattern of Co_3O_4 NPs with [110] plane in the Co_3O_4/graphene composite, indicative of the well-textured and single-crystalline nature of Co_3O_4 NPs.

less agglomeration for graphene sheets in composite. All of the other diffraction peaks can be ascribed to the well-crystallized Co_3O_4 with a face-centered cubic (fcc, *Fd*3*m* (227), $a = 0.808$ nm) structure (JCPDS No. 42-1467).[8] These results indicate that the composite consists of disorderedly stacked graphene sheets and well-crystallized Co_3O_4.

To determine the chemical composition of Co_3O_4/graphene composite, X-ray photoelectron spectroscopy (XPS) measurements were carried out in the region of 0−1300 eV (Figure 2b). The Co 2p XPS spectra of the composite exhibit two peaks at 795.6 and 780.2 eV, corresponding to the Co $2p_{1/2}$ and Co $2p_{3/2}$ spin−orbit peaks of Co_3O_4 (Figure 2c).[54] The presence of Co_3O_4 can be further confirmed by the O 1s XPS peak at 530.1 eV, which corresponds to the oxygen species in the Co_3O_4 phase (Figure 2d).[54] The C 1s (284.6 eV) peak observed is related to graphitic carbon in graphene, and the small O 1s peak at 532.0 eV in the spectrum indicates the presence of residual oxygen-containing groups (such as −OH and −COOH) bonded with C atoms in graphene (Figure 2d).[55] It is important to note that the C/O ratio for graphene in the composite was estimated to be 55.0 after subtracting the oxygen species involved in O−Co chemical bonds of Co_3O_4 in the composite, which is much higher than that (10.7) of the as-prepared graphene. It is considered that the decreased oxygen-containing groups are possibly involved in the formation of Co_3O_4 anchored on the surface of graphene sheets, and a further study is required to elucidate this point in the future. Such a high C/O ratio of the graphene sheets implies a good electronic conductivity, which may enable the graphene sheets to serve as the conductive channels between Co_3O_4 NPs, and is favorable for stabilizing the electronic and ionic conductivity consequently.

Figure 3 shows scanning electron microscopy (SEM) and transmission electron microscopy (TEM) images of the as-prepared Co_3O_4/graphene composite. It can be seen from Figure 3a and Figure S3 (Supporting Information) that small Co_3O_4 NPs are closely anchored on the surface of graphene sheets. Figure 3b,c shows the TEM images of the as-prepared Co_3O_4/graphene composite, from which it can be seen that the Co_3O_4 NPs have a size of 10−30 nm and are homogeneously anchored on the thin graphene layers. The selected area electron diffraction (SAED) pattern (inset in Figure 3c) and high-resolution TEM (HRTEM) image (Figure 3d and Figure S4) clearly demonstrate the well-textured and single-crystalline nature of Co_3O_4 NPs in the Co_3O_4/graphene composite, consistent with the XRD results. It should be emphasized that, without the presence of graphene, no Co_3O_4 NPs were formed at the same conditions as those for the preparation of the Co_3O_4/graphene composite (Figure S5). This result strongly indicates that the presence of graphene plays an essential role in the formation of homogeneous Co_3O_4 NPs. Another phenomenon is that, even after a long time of sonication during the preparation of the TEM specimen, the NPs are still strongly anchored on the surface of graphene sheets with a high density, as shown in Figure 3b,c, suggesting the strong interaction between NPs and graphene sheets. We believe that such interaction combined with good mechanical flexibility of graphene sheets pre-

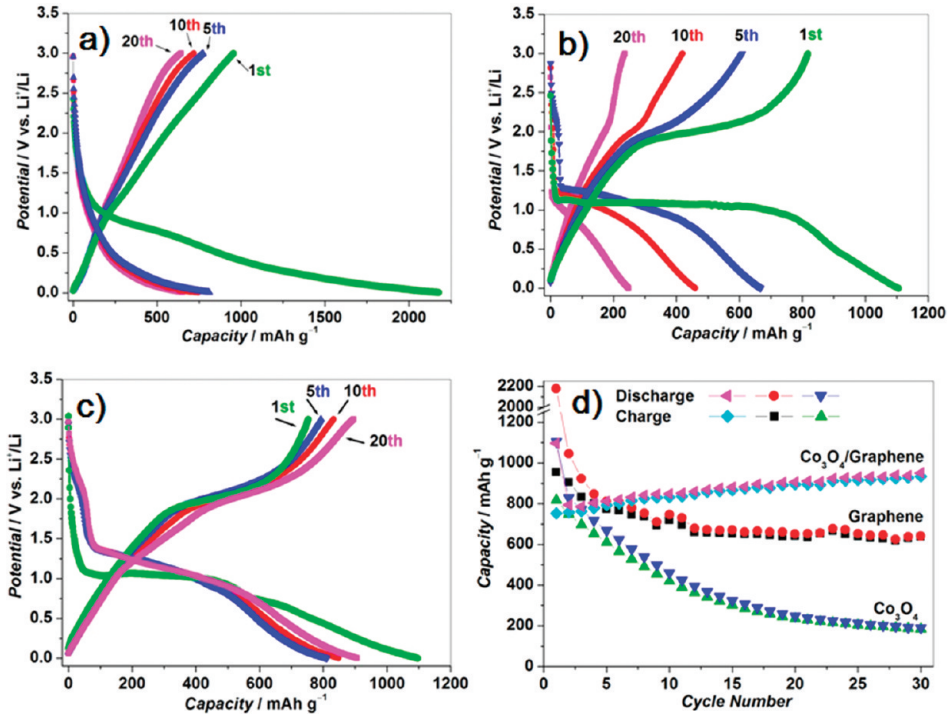

Figure 4. Galvanostatic charge−discharge curves of (a) graphene, (b) Co_3O_4, and (c) the Co_3O_4/graphene composite cycled at the 1st, 5th, 10th, and 20th between 3 and 0.01 V (*vs* Li^+/Li) at a current density of 50 mA g^{-1}. (d) Comparison of the cycling performance of graphene, Co_3O_4, and the Co_3O_4/graphene composite.

vents the agglomeration of NPs to large particles, as shown in Figure S5 (Supporting Information), in the presence of graphene sheets. In addition, the strong anchoring of Co_3O_4 NPs on graphene sheets enables fast electron transport through the underlying graphene layers to NPs to improve the electrochemical performance.[40] On the other hand, the NPs on the surface of graphene sheets can act as spacers to efficiently prevent the closely restacking of graphene sheets, avoiding/weakening the loss of their high active surface area.[56]

The electrochemical performance of the as-prepared Co_3O_4/graphene composite was first evaluated by galvanostatic charge/discharge cycling at a current density of 50 mA g^{-1}. For comparison, we also present the result of pure graphene (Figure 4a) and Co_3O_4 (Figure 4b) prepared by the same procedure under the same electrochemical conditions. Figure 4b,c shows the charge/discharge profiles of the Co_3O_4 and Co_3O_4/graphene composite electrodes in the 1st, 5th, 10th, and 20th cycles. In the first discharge step, both of them present a long voltage plateau at 1.06 V for the Co_3O_4/graphene composite and 1.10 V for Co_3O_4, followed by a sloping curve down to the cutoff voltage of 0.01 V, indicative of typical characteristics of voltage trends for the Co_3O_4 electrode.[10] However, no obvious voltage plateau was observed for graphene (Figure 4a).[38] The first discharge and charge capacities are 2179 and 955 mAh g^{-1} for graphene, 1105 and 817 mAh g^{-1} for Co_3O_4, and 1097 and ~753 mAh g^{-1} for Co_3O_4/graphene composite electrodes. Compared to the theoretical capacity of bulk Co_3O_4 (890 mAh g^{-1}) and graphite (372 mAh g^{-1}), the extra discharge capacity of the Co_3O_4/graphene composite may be attributed to the larger electrochemical active surface area of graphene and/or grain boundary area of the nanosized Co_3O_4 particles.[30,38] The initial capacity loss may result from the incomplete conversion reaction and irreversible lithium loss due to the formation of a solid electrolyte interphase (SEI) layer.[10] Since the second cycle, however, the Co_3O_4/graphene composite electrode presents much better electrochemical lithium storage performance than Co_3O_4 electrode. After five discharge/charge cycles, it exhibits a high reversible capacity of ~800 mAh g^{-1}. The Coulombic efficiency rapidly rises from 68.6% in the first cycle to 97.6% in the fifth one and then remains above 98% in the following cycles (Figure 4c). In contrast, the reversible capacity of the Co_3O_4 electrode rapidly drops to 609 mAh g^{-1} with a low Coulombic efficiency of 91.3% after the fifth cycle and then gradually increases to 95.1% for the 20th cycle (Figure 4b). Compared to the Co_3O_4/graphene composite and Co_3O_4 electrodes, the graphene electrode shows larger discharge/charge capacity in the first cycle but suffers from a lower initial Coulombic efficiency (only 43.8%) and fast reversible capacity fading (773 mAh g^{-1} for the fifth cycle, 642 mAh g^{-1} for the 20th cycle, Figure 4a). More importantly, the Co_3O_4/graphene composite exhibits a much better cycling performance than graphene and Co_3O_4 (Figure 4d). It can be seen that the reversible capacity of graphene and Co_3O_4 decreases from 955 to 638 mAh g^{-1} and from 817 to only 184 mAh g^{-1}, re-

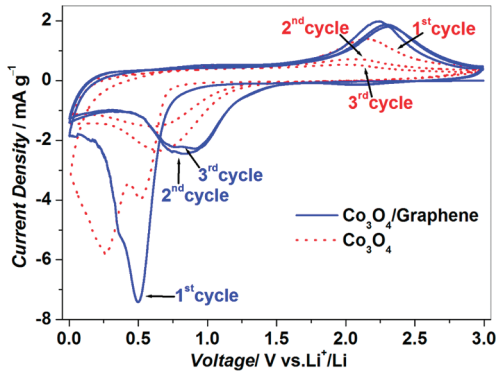

Figure 5. Cyclic voltammograms of the Co_3O_4/graphene composite (solid line) and Co_3O_4 (dotted line) at a scanning rate of 1 mV s^{-1}.

spectively, up to 30 cycles. In contrast, the reversible capacity of the Co_3O_4/graphene composite slightly increases with cycling and reaches ~935 mAh g^{-1} after 30 cycles. From Figure 4d and Figure S6 (Supporting Information), it is important to note that there is a strong synergistic effect between Co_3O_4 NPs and graphene sheets in the composite, which becomes much more apparent with cycling and plays a central role in the excellent cyclic performance of the Co_3O_4/graphene composite.

Figure 5 presents cyclic voltammograms (CV) of the as-prepared Co_3O_4/graphene composite and Co_3O_4 electrodes. In the first cycle, two cathodic peaks were observed at 0.50 and 0.36 V for the Co_3O_4/graphene composite and at 0.51 and 0.26 V for Co_3O_4, corresponding to a multistep electrochemical reduction (lithiation) reaction of Co_3O_4 with Li.[8] The observed main anodic peak at 2.24 V for the Co_3O_4/graphene composite and at 2.15 V for Co_3O_4 is ascribed to the oxidation (delithiation) reaction of Co_3O_4. The formation of Co and Li_2O and the re-formation of Co_3O_4 can be described by the electrochemical conversion reaction:[8,10]

$$Co_3O_4 + 8Li \underset{\text{charge}}{\overset{\text{discharge}}{\rightleftharpoons}} 4Li_2O + 3Co$$

The cathodic peak below 0.8 V for Co_3O_4 is broader than that of Co_3O_4/graphene composite partly due to the electrolyte decomposition and formation of the SEI layer.[10,41] The weak but discriminable reduction and oxidation peaks at 0.045 and 0.21 V/1.0 V, respectively, are observed for the composite electrode but are absent for Co_3O_4 due to the insertion/extraction of Li into/from graphene, suggesting that the graphene in the Co_3O_4/graphene composite is also electroactive for lithium storage.[41] In the second cycle, the main reduction peak is shifted to 0.83 V for the Co_3O_4/graphene composite and to 0.66 V for Co_3O_4. The peak intensity and integral areas of the third cycle are close to that of the second one for Co_3O_4/graphene but are obviously decreased for Co_3O_4 (Figure 5). These results indicate that the electrochemical reversibility of Co_3O_4/graphene is gradually built after the initial cycle and much better than that for Co_3O_4.

In addition, the Co_3O_4/graphene composite exhibits much better rate capability compared to the Co_3O_4 electrode operated at various rates between 50 and 500 mA g^{-1} (Figure 6a,b). For example, the Co_3O_4/graphene composite keeps a reversible capacity of 800 mAh g^{-1} after the 10th cycle at a current density of 50 mA g^{-1}, whereas the reversible capacity of the Co_3O_4 electrode rapidly drops from 759 to 541 mAh g^{-1}. The following reversible capacity of the Co_3O_4/graphene composite and Co_3O_4 electrodes at other various rates is 715 and 239 mAh g^{-1} for the 20th cycle at 150 mA g^{-1}, 631 and 122 mAh g^{-1} for the 30th cycle at 250 mA g^{-1}, and 484 and 53 mAh g^{-1} for the 40th cycle at 500 mA g^{-1}, respectively, with ~66.2% (only ~7.1% for Co_3O_4) of the initial reversible capacity. Moreover, when the rate returns to the initial 50 mA g^{-1} after 40 cycles, the composite electrode recovers its original capacity or even a little bit higher (767 mAh g^{-1} for the 50th cycle), but the Co_3O_4 electrode cannot go back, as illustrated in Figure 6a,b.

A rough comparison indicates that the reversible capacity (935 mAh g^{-1}) of the Co_3O_4/graphene composite is much better than those previously reported, such as carbon nanofiber/Co_3O_4[28,29] and mesoporous carbon/Co_3O_4[30] composites, and some unique Co_3O_4 nano/microstrucutres of NPs,[8] nanotubes,[8] nanorods,[8] nanowires,[27] octahedral cages,[35] and plates.[10] The increase of cyclic capacity is different from other appeal-

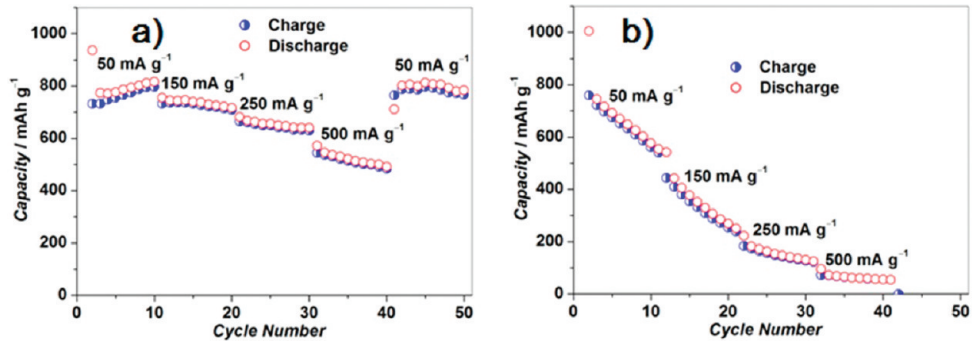

Figure 6. Rate capability of the Co_3O_4/graphene composite (a) and Co_3O_4 (b) at various current densities between 50 and 500 mA g^{-1}.

ing strategies for improving electrochemical performance of the Co_3O_4 system,[8,27,30,35] demonstrating the excellent cyclic performance of Co_3O_4/graphene composite. The initial Coulombic efficiency (68.6%) of the Co_3O_4/graphene composite is not prominent, but still higher than those of mesoporous carbon/Co_3O_4 (55%),[30] NPs (55.2%),[8] nanotubes (58.8%),[8] and nanorods (57.8%).[8] Of importance is that more than ~98% of Coulombic efficiency was observed after the fifth cycle, indicative of high charge/discharge reversibility of the Co_3O_4/graphene composite electrode.

Combining the highly reversible capacity, excellent cyclic performance, and high Coulombic efficiency with good rate capability, we believe that such composites of graphene anchored with Co_3O_4 NPs are a good candidate as anode material of high-performance LIBs. The superior Li-battery performance of the Co_3O_4/graphene composite electrode can be explained as follows: (i) Graphene sheets act as flexible two-dimensional carbon supports for homogeneous anchoring of Co_3O_4 NPs. The graphene sheets in the obtained composite not only provide an elastic buffer space to accommodate the volume expansion/contraction of Co_3O_4 NPs during Li insertion/extraction process but also efficiently prevent the aggregation of Co_3O_4 NPs and the cracking or crumbling of electrode material upon continuous cycling, thus maintaining large capacity, good Coulombic efficiency, high rate capability and cycling stability.[40] (ii) The graphene sheets in the composite have a good electrical conductivity[57] and serve as the conductive channels between Co_3O_4 NPs, which decreases the inner resistance of LIBs and is favorable for stabilizing the electronic and ionic conductivity, therefore leading to a higher specific capacity.[52] (iii) Li-ion diffusion strongly depends on the transport length and accessible sites on the surface of active materials.[52] Therefore, it is expected that the Co_3O_4 NPs as well as ultrathin graphene sheets in the nanocomposite offer improved energy storage capacity, Coulombic efficiency, and better cycling stability due to the large electrode/electrolyte contact area, short path length for Li^+ transport, and good stability for nanostructured electrodes.[3,52] (iv) The presence of Co_3O_4 NPs between graphene sheets effectively prevents the agglomeration of graphene sheets and consequently keeps their high active surface area, which is favorable for increasing the Li storage capacity of graphene in the composite. On the basis of the above analyses, it is concluded that the synergetic effect between conducting graphene sheets and Co_3O_4 NPs is responsible for the excellent electrochemical performance of the overall electrode *via* the maximum utilization of electrochemically active graphene and nanosized Co_3O_4.

CONCLUSIONS

We developed a facile strategy to synthesize a composite of electrically conductive graphene anchored with Co_3O_4 NPs as an advanced anode material for high-performance LIBs. The Co_3O_4 NPs obtained are 10−30 nm in size and homogeneously anchored on graphene as spacers to keep the neighboring graphene sheets separated. Moreover, the flexible structure of two-dimensional graphene sheets and the strong interaction between Co_3O_4 NPs and graphene sheets in Co_3O_4/graphene composite are beneficial for efficiently preventing volume expansion/contraction and aggregation of Co_3O_4 during Li charge/discharge process. Therefore, such a composite is capable of effectively utilizing the good conductivity, high surface area, mechanical flexibility, and good electrochemical performance of graphene as well as the large electrode/electrolyte contact area, short path length for Li^+ transport, and good stability for nanostructured Co_3O_4 particles. As a result, the Co_3O_4/graphene composite exhibits a large reversible capacity (~935 mAh g^{-1} after 30 cycles), excellent cyclic performance, high Coulombic efficiency (above ~98%), and good rate capability, highlighting the advantages of anchoring of NPs on graphene sheets for the maximum utilization of electrochemically active Co_3O_4 NPs and graphene for energy storage applications in high-performance LIBs.

EXPERIMENTAL SECTION

Synthesis of the Co_3O_4/Graphene Composite. The graphene sheets (≤3 layers) used were synthesized by chemical exfoliation of flake graphite powder (500 mesh) and reduction as previously reported[57] and have a C/O ratio of 10.7. The Co_3O_4/graphene composite was prepared as follows. First, 100 mg of graphene was dispersed in 100 mL of isopropyl alcohol−water (1:1, v/v) solution by sonication for 0.5 h and transferred into a three-necked round-bottom flask under argon flow. An appropriate amount of inorganic salts, $Co(NO_3)_2 \cdot 6H_2O$, followed by ammonia solution ($NH_3 \cdot H_2O$, 25 wt %), was slowly added into the above suspension and then stirred for several hours under an argon flow to ensure complete reaction. The obtained $Co(OH)_2$/graphene composite precursor was filtered and dried under vacuum at 70 °C. Finally, the $Co(OH)_2$/graphene composite precursor was calcined at 450 °C in air for 2 h to obtain the Co_3O_4/graphene composite. According to thermogravimetry/differentiate thermogravimetry (TG/DTG) analyses (Figure S7 in Supporting Information), the weight percentage of Co_3O_4 and graphene in the Co_3O_4/graphene composite was estimated to be ~75.4 and ~24.6 wt %, respectively. For comparison, Co_3O_4 particles were also prepared in the same conditions but without the presence of graphene.

Materials Characterizations. The Co_3O_4/graphene composites were characterized by XRD (D/max 2400 with Cu Kα radiation), XPS (Escalab 250, Al Kα), SEM (Nova Nano 430), and HRTEM (JEOL JEM 2010, 200 kV and Tecnai F30, 300 kV), and TG/DTG (Netzsch-STA 449C, measured from 30 to 800 °C at a heating rate of 10 °C/min in air). The Co_3O_4 particles prepared without the presence of graphene were characterized by XRD, SEM, and TEM.

Electrochemical Measurements. The working electrodes were prepared by mixing 80 wt % active material (Co_3O_4/graphene composite, Co_3O_4), 12 wt % acetylene black (Super-P), and 8 wt % polyvinylidene fluoride (PVDF, 5 wt %) binder dissolved in

N-methyl-2-pyrrolidinone. After coating the above slurries on Cu foils, the electrodes were dried at 120 °C in vacuum for 2 h to remove the solvent before pressing. Then the electrodes were cut into disks (12 mm in diameter) and dried at 100 °C for 24 h in vacuum. For graphene, the electrode was prepared by the same procedure with 70 wt % graphene, 10 wt % acetylene black, and 20 wt % PVDF. Electrochemical measurements were carried out *via* CR2032 (3 V) coin-type cell with lithium metal as the counter/reference electrode, Celgard 2400 membrane separator, and 1 M $LiPF_6$ electrolyte solution dissolved in a mixture of ethylene carbonate (EC) and dimethyl carbonate (DMC) (EC/DMC, 1:1 v/v). The cells were assembled in an argon-filled glovebox. CV measurements were carried out using a Solartron 1287 electrochemical workstation at a scanning rate of 1 mV s^{-1}. Galvanostatic charge−discharge cycles were tested by LAND CT2001A electrochemical workstation at various current densities of 50−500 mA g^{-1} between 3 and 0.01 V *vs* Li^+/Li at room temperature.

Acknowledgment. This work was supported by Ministry of Science and Technology of China (No. 2006CB932703), National Science Foundation of China (Nos. 50872136 and 50921004), and Chinese Academy of Sciences (No. KJCX2-YW-231).

Supporting Information Available: XRD patterns of the Co_3O_4, graphene sheets, and Co_3O_4/graphene composite, SEM and TEM images of Co_3O_4, HRTEM image and TG/DTG analysis of Co_3O_4/graphene composite, and the analysis of the maximum utilization of electrochemically active graphene and Co_3O_4 NPs in composite. This material is available free of charge *via* the Internet at http://pubs.acs.org.

REFERENCES AND NOTES

1. Winter, M.; Besenhard, J. O.; Spahr, M. E.; Novak, P. Insertion Electrode Materials for Rechargeable Lithium Batteries. *Adv. Mater.* **1998**, *10*, 725–763.
2. Liu, C.; Li, F.; Ma, L. P.; Cheng, H. M. Advanced Materials for Energy Storage. *Adv. Mater.* **2010**, *22*, 28–62.
3. Guo, Y. G.; Hu, J. S.; Wan, L. J. Nanostructured Materials for Electrochemical Energy Conversion and Storage Devices. *Adv. Mater.* **2008**, *20*, 2878–2887.
4. Kaskhedikar, N. A.; Maier, J. Lithium Storage Ion Carbon Nanostructures. *Adv. Mater.* **2009**, *21*, 2664–2680.
5. Meduri, P.; Pendyala, C.; Kumar, V.; Sumanasekera, G. U.; Sunkara, M. K. Hybrid Tin Oxide Nanowires as Stable and High Capacity Anodes for Li-Ion Batteries. *Nano Lett.* **2009**, *9*, 612–616.
6. Hu, Y. S.; Kienle, L.; Guo, Y. G.; Maier, J. High Lithium Electroactivity of Nanometer-Sized Rutile TiO_2. *Adv. Mater.* **2006**, *18*, 1421–1426.
7. Wu, C. Z.; Yin, P.; Zhu, X.; OuYang, C. Z.; Xie, Y. Synthesis of Hematite (α-Fe_2O_3) Nanorods: Diameter-Size and Shape Effects on Their Applications in Magnetism, Lithium Ion Battery, and Gas Sensors. *J. Phys. Chem. B* **2006**, *110*, 17806–17812.
8. Li, W. Y.; Xu, L. N.; Chen, J. Co_3O_4 Nanomaterials in Lithium-Ion Batteries and Gas Sensors. *Adv. Funct. Mater.* **2005**, *15*, 851–857.
9. Du, N.; Zhang, H.; Chen, B.; Wu, J. B.; Ma, X. Y.; Liu, Z. H.; Zhang, Y. Q.; Yang, D.; Huang, X. H.; Tu, J. P. Porous Co_3O_4 Nanotubes Derived from $Co_4(Co)_{12}$ Clusters on Carbon Nanotube Templates: A Highly Efficient Material for Li-Battery Applications. *Adv. Mater.* **2007**, *19*, 4505–4509.
10. Yao, W. L.; Yang, J.; Wang, J. L.; Nuli, Y. Multilayered Cobalt Oxide Platelets for Negative Electrode Material of a Lithium-Ion Battery. *J. Electrochem. Soc.* **2008**, *155*, A903–A908.
11. Varghese, B.; Reddy, M. V.; Yanwu, Z.; Lit, C. S.; Hoong, T. C.; Rao, G. V. S.; Chowdari, B. V. R.; Wee, A. T. S.; Lim, C. T.; Sow, C. H. Fabrication of NiO Nanowall Electrodes for High Performance Lithium Ion Battery. *Chem. Mater.* **2008**, *20*, 3360–3367.
12. Zhao, J. Z.; Tao, Z. L.; Liang, J.; Chen, J. Facile Synthesis of Nanoporous γ-MnO_2 Structures and Their Application in Rechargeable Li-Ion Batteries. *Cryst. Growth Des.* **2008**, *8*, 2799–2805.
13. Whittingham, M. S. Chemistry of Intercalation Compounds—Metal Guests in Chalcogenide Hosts. *Prog. Solid State Chem.* **1978**, *12*, 41–99.
14. Scrosati, B. Lithium Rocking Chair Batteries—An Old Concept. *J. Electrochem. Soc.* **1992**, *139*, 2776–2781.
15. Gopalakrishnan, J. Insertion/Extraction of Lithium and Sodium in Transition Metal Oxides and Chalcogenides. *Bull. Mater. Sci.* **1985**, *7*, 201–214.
16. Seo, J. W.; Jang, J. T.; Park, S. W.; Kim, C. J.; Park, B. W.; Cheon, J. W. Two-Dimensional SnS_2 Nanoplates with Extraordinary High Discharge Capacity for Lithium Ion Batteries. *Adv. Mater.* **2008**, *20*, 4269–4273.
17. Rowsell, J. L. C.; Pralong, V.; Nazar, L. F. Layered Lithium Iron Nitride: A Promising Anode Material for Li-Ion Batteries. *J. Am. Chem. Soc.* **2001**, *123*, 8598–8599.
18. Novak, P.; Muller, K.; Santhanam, K. S. V.; Haas, O. Electrochemically Active Polymers for Rechargeable Batteries. *Chem. Rev.* **1997**, *97*, 207–281.
19. Besenhard, J. O.; Yang, J.; Winter, M. Will Advanced Lithium-Alloy Anodes Have a Chance in Lithium-Ion Batteries. *J. Power Sources* **1997**, *68*, 87–90.
20. Ma, H.; Cheng, F. Y.; Chen, J.; Zhao, J. Z.; Li, C. S.; Tao, Z. L.; Liang, J. Nest-like Silicon Nanospheres for High-Capacity Lithium Storage. *Adv. Mater.* **2007**, *19*, 4067–4070.
21. Hassoun, J.; Panero, S.; Simon, P.; Taberna, P. L.; Scrosati, B. High-Rate, Long-Life Ni−Sn Nanostructured Electrodes for Lithium-Ion Batteries. *Adv. Mater.* **2007**, *19*, 1632–1635.
22. Derrien, G.; Hassoun, J.; Panero, S.; Scrosati, B. Nanostructured Sn−C Composite as an Advanced Anode Material in High-Performance Lithium-Ion Batteries. *Adv. Mater.* **2007**, *19*, 2336–2340.
23. Yu, Y.; Chen, C. H.; Shi, Y. A Tin-Based Amorphous Oxide Composite with a Porous, Spherical, Multideck-Cage Morphology as a Highly Reversible Anode Material for Lithium-Ion Batteries. *Adv. Mater.* **2007**, *19*, 993–997.
24. Zhang, H. X.; Feng, C.; Zhai, Y. C.; Jiang, K. L.; Li, Q. Q.; Fan, S. S. Cross-Stacked Carbon Nanotube Sheets Uniformly Loaded with SnO_2 Nanoparticles: A Novel Binder-Free and High-Capacity Anode Material for Lithium-Ion Batteries. *Adv. Mater.* **2009**, *21*, 2299–2304.
25. Hassoun, J.; Derrien, G.; Panero, S.; Scrosati, B. A Nanostructured Sn−C Composite Lithium Battery Electrode with Unique Stability and High Electrochemical Performance. *Adv. Mater.* **2008**, *20*, 3169–3175.
26. Cui, L. F.; Yang, Y.; Hsu, C. M.; Cui, Y. Carbon−Silicon Core−Shell Nanowires as High Capacity Electrode for Lithium Ion Batteries. *Nano Lett.* **2009**, *9*, 3370–3374.
27. Li, Y. G.; Tan, B.; Wu, Y. Y. Mesoporous Co_3O_4 Nanowire Arrays for Lithium Ion Batteries with High Capacity and Rate Capability. *Nano Lett.* **2008**, *8*, 265–270.
28. Yao, W. L.; Wang, J. L.; Yang, J.; Du, G. D. Novel Carbon Nanofiber-Cobalt Oxide Composites for Lithium Storage with Large Capacity and High Reversibility. *J. Power Sources* **2008**, *176*, 369–372.
29. Yao, W. L.; Yang, J.; Wang, J. L.; Tao, L. A. Synthesis and Electrochemical Performance of Carbon Nanofiber-Cobalt Oxide Composites. *Electrochim. Acta* **2008**, *53*, 7326–7330.
30. Liu, H. J.; Bo, S. H.; Cui, W. J.; Li, F.; Wang, C. X.; Xia, Y. Y. Nano-Sized Cobalt Oxide/Mesoporous Carbon Sphere Composites as Negative Electrode Material for Lithium-Ion Batteries. *Electrochim. Acta* **2008**, *53*, 6497–6503.
31. Su, D. S.; Schlogl, R. Nanostructured Carbon and Carbon Nanocomposites for Electrochemical Energy Storage Applications. *ChemSusChem* **2010**, *3*, 136–168.
32. Zhi, L. J.; Hu, Y. S.; El Hamaoui, B.; Wang, X.; Lieberwirth, I.; Kolb, U.; Maier, J.; Mullen, K. Precursor-Controlled Formation of Novel Carbon/Metal and Carbon/Metal Oxide Nanocomposites. *Adv. Mater.* **2008**, *20*, 1727–1731.
33. Liu, B.; Zhang, X. B.; Shioyama, H.; Mukai, T.; Sakai, T.; Xu, Q. Converting Cobalt Oxide Subunits in Cobalt Metal-Organic Framework into Agglomerated Co_3O_4 Nanoparticles as an Electrode Material for Lithium Ion Battery. *J. Power Sources* **2010**, *195*, 857–861.

34. Zhang, H.; Wu, J. B.; Zhai, C. X.; Ma, X. Y.; Du, N.; Tu, J. P.; Yang, D. R. From Cobalt Nitrate Carbonate Hydroxide Hydrate Nanowires to Porous Co_3O_4 Nanorods for High Performance Lithium-Ion Battery Electrodes. *Nanotechnology* **2008**, *19*, 035711.
35. Wang, X.; Yu, L. J.; Wu, X. L.; Yuan, F. L.; Guo, Y. G.; Ma, Y.; Yao, J. N. A. Synthesis of Single-Crystalline Co_3O_4 Octahedral Cages with Tunable Surface Aperture and Their Lithium Storage Properties. *J. Phys. Chem. C* **2009**, *113*, 15553–15558.
36. Yoo, E.; Kim, J.; Hosono, E.; Zhou, H.; Kudo, T.; Honma, I. Large Reversible Li Storage of Graphene Nanosheet Families for Use in Rechargeable Lithium Ion Batteries. *Nano Lett.* **2008**, *8*, 2277–2282.
37. Wang, G. X.; Shen, X. P.; Yao, J.; Park, J. Graphene Nanosheets for Enhanced Lithium Storage in Lithium Ion Batteries. *Carbon* **2009**, *47*, 2049–2053.
38. Pan, D. Y.; Wang, S.; Zhao, B.; Wu, M. H.; Zhang, H. J.; Wang, Y.; Jiao, Z. Li Storage Properties of Disordered Graphene Nanosheets. *Chem. Mater.* **2009**, *21*, 3136–3142.
39. Lian, P.; Zhu, X.; Liang, S.; Li, Z.; Yang, W.; Wang, H. Large Reversible Capacity of High Quality Graphene Sheets as an Anode Material for Lithium-Ion Batteries. *Electrochim. Acta* **2010**, *55*, 3909–3914.
40. Paek, S. M.; Yoo, E.; Honma, I. Enhanced Cyclic Performance and Lithium Storage Capacity of SnO_2/Graphene Nanoporous Electrodes with Three-Dimensionally Delaminated Flexible Structure. *Nano Lett.* **2009**, *9*, 72–75.
41. Yao, J.; Shen, X. P.; Wang, B.; Liu, H. K.; Wang, G. X. In Situ Chemical Synthesis of SnO_2-Graphene Nanocomposite as Anode Materials for Lithium-Ion Batteries. *Electrochem. Commun.* **2009**, *11*, 1849–1852.
42. Wang, G. X.; Wang, B.; Wang, X. L.; Park, J.; Dou, S. X.; Ahn, H.; Kim, K. Sn/Graphene Nanocomposite with 3D Architecture for Enhanced Reversible Lithium Storage in Lithium Ion Batteries. *J. Mater. Chem.* **2009**, *19*, 8378–8384.
43. Chou, S. L.; Wang, J. Z.; Choucair, M.; Liu, H. K.; Stride, J. A.; Dou, S. X. Enhanced Reversible Lithium Stroage in a Nanosize Silicon/Graphene Composite. *Electrochem. Commun.* **2010**, *12*, 303–306.
44. Wang, D. H.; Choi, D. W.; Li, J.; Yang, Z. G.; Nie, Z. M.; Kou, R.; Hu, D. H.; Wang, C. M.; Saraf, L. V.; Zhang, J. G.; Aksay, I. A.; Liu, J. Self-Assembled TiO_2-Graphene Hybrid Nanostructures for Enhanced Li-Ion Insertion. *ACS Nano* **2009**, *3*, 907–914.
45. Ji, F.; Li, Y. L.; Feng, J. M.; Su, D.; Wen, Y. Y.; Feng, Y.; Hou, F. Electrochemical Performance of Graphene Nanosheets and Ceramic Composites as Anodes for Lithium Batteries. *J. Mater. Chem.* **2009**, *19*, 9063–9067.
46. Novoselov, K. S.; Geim, A. K.; Morozov, S. V.; Jiang, D.; Zhang, Y.; Dubonos, S. V.; Grigorieva, I. V.; Firsov, A. A. Electric Field Effect in Atomically Thin Carbon Films. *Science* **2004**, *306*, 666–669.
47. Novoselov, K. S.; Jiang, D.; Schedin, F.; Booth, T. J.; Khotkevich, V. V.; Morozov, S. V.; Geim, A. K. Two-Dimensional Atomic Crystals. *Proc. Natl. Acad. Sci. U.S.A.* **2005**, *102*, 10451–10453.
48. Novoselov, K. S.; Geim, A. K.; Morozov, S. V.; Jiang, D.; Katsnelson, M. I.; Grigorieva, I. V.; Dubonos, S. V.; Firsov, A. A. Two-Dimensional Gas of Massless Dirac Fermions in Graphene. *Nature* **2005**, *438*, 197–200.
49. Geim, A. K.; Novoselov, K. S. The Rise of Graphene. *Nat. Mater.* **2007**, *6*, 183–191.
50. Geim, A. K. Graphene: Status and Prospects. *Science* **2009**, *324*, 1530–1534.
51. Kamat, P. V. Graphene-Based Nanoarchitectures. Anchoring Semiconductor and Metal Nanoparticles on a Two-Dimensional Carbon Support. *J. Phys. Chem. Lett.* **2010**, *1*, 520–527.
52. Jiang, C. H.; Hosono, E.; Zhou, H. S. Nanomaterials for Lithium Ion Batteries. *Nano Today* **2006**, *1*, 28–33.
53. Wang, G. X.; Yang, J.; Park, J.; Gou, X. L.; Wang, B.; Liu, H.; Yao, J. Facile Synthesis and Characterization of Graphene Nanosheets. *J. Phys. Chem. C* **2008**, *112*, 8192–8195.
54. Varghese, B.; Hoong, T. C.; Yanwu, Z.; Reddy, M. V.; Chowdari, B. V. R.; Wee, A. T. S.; Vincent, T. B. C.; Lim, C. T.; Sow, C. H. Co_3O_4 Nanostructures with Different Morphologies and Their Field-Emission Properties. *Adv. Funct. Mater.* **2007**, *17*, 1932–1939.
55. Schniepp, H. C.; Li, J. L.; McAllister, M. J.; Sai, H.; Herrera-Alonso, M.; Adamson, D. H.; Prud'homme, R. K.; Car, R.; Saville, D. A.; Aksay, I. A. Functionalized Single Graphene Sheets Derived from Splitting Graphite Oxide. *J. Phys. Chem. B* **2006**, *110*, 8535–8539.
56. Si, Y. C.; Samulski, E. T. Exfoliated Graphene Separated by Platinum Nanoparticles. *Chem. Mater.* **2008**, *20*, 6792–6797.
57. Wu, Z. S.; Ren, W.; Gao, L.; Liu, B.; Jiang, C.; Cheng, H. M. Synthesis of High-Quality Graphene with a Pre-determined Number of Layers. *Carbon* **2009**, *47*, 493–499.